J. Plasma Physics (2012), vol. 78, part 4, pp. 363–371. © Cambridge University Press 2012
doi:10.1017/S0022377812000098

Controlled ionization-induced injection by tailoring the gas-density profile in laser wakefield acceleration

MING ZENG[1], NASR A. M. HAFZ[1], KAZUHISA NAKAJIMA[1,2,3], LI-MING CHEN[1,4], WEI LU[5,7], WARREN B. MORI[6,7], ZHENG-MING SHENG[1,4] and JIE ZHANG[1,4]

[1]Key Laboratory for Laser Plasmas (Ministry of Education), Shanghai Jiao Tong University, Shanghai 200240, China (zmsheng@sjtu.edu.cn)
[2]High Energy Accelerator Research Organization, 1-1 Oho, Tsukuba, Ibaraki 305-0081, Japan
[3]Shanghai Institute of Optics and Fine Mechanics, CAS, Shanghai 201800, China
[4]Beijing National Laboratory of Condensed Matter Physics, Institute of Physics, CAS, Beijing 100190, China
[5]Department of Engineering Physics, Tsinghua University, Beijing 100084, China
[6]Department of Electrical Engineering, UCLA, Los Angeles, CA 90095, USA
[7]Department of Physics and Astronomy, UCLA, Los Angeles, CA 90095, USA

(Received 27 October 2011; revised 5 January 2012; accepted 6 January 2012; first published online 7 February 2012)

Abstract. Ionization-induced injection into a laser-driven wakefield is studied using $2\frac{1}{2}$D OSIRIS simulations. A laser propagates into a gas mixture of 99.5% helium and 0.5% nitrogen with gas density of each rising linearly from 0 to a peak, after which these remain constant. Simulations show that the process can be controlled by varying the scale length of an up-ramp, the laser intensity, and the maximum plasma density. The injection process is controlled by the bubble radius decreasing as laser propagates up the density gradient and laser self-focusing in the flat-top region. A beam with a central energy of 350 MeV and an energy spread (FWHM) of 1.62% was obtained for an up-ramp length of 135 μm, a normalized vector potential of 2, and a density of 7×10^{18} cm^{-3} (assuming a 0.8 μm wavelength laser).

1. Introduction

Particle accelerators are powerful tools used by physicists to answer the most basic questions about the nature of the universe. Accelerators not only bring us new knowledge about our universe but also provide excellent tools for industrial, medical, and other applications. Accelerators based on conventional radio-frequency (RF) technologies are expensive and require long accelerating structures, which can be as long as tens of kilometres to produce high energy particles. The main limitation of the RF-based accelerator is the maximum achievable acceleration gradient, which is limited by the material breakdowns to a few tens of mega electron volts (MeV) per meter. The recent progresses in the laser wakefield acceleration (LWFA) scheme make it a promising technology for the next generation accelerators based on the state-of-the-art compact laser technologies. In LWFA, acceleration gradients up to hundreds of GeV per meter (Tajima and Dawson 1979) are achievable, enabling much more compact and low-cost, high-energy accelerators. Until recently, the limitation of a LWFA-produced electron beam was its large energy spread (Malka et al. 2002). However, a breakthrough in this field was reported in 2004, when three experimental groups simultaneously reported monoenergetic beam generation from LWFA (Faure et al. 2004; Geddes et al. 2004; Mangles et al. 2004) with energy spread of the order of 10%, and another group published 3D simulation results for related laser parameters (Tsung et al. 2004). However, the 10% level of beam energy spread is still far from satisfactory for many applications such as free electron lasers (FEL).

One of the most important issues in LWFA is how to inject electrons into the laser wakefield. Injection means placing electrons into the focusing and accelerating phase with proper velocity so that they can be accelerated up to dephasing distances (Esarey et al. 2009). Thus, the injection mechanism is critical and determines the energy spread and emittance of electron beam. Some known injection mechanisms are self-injection (Faure et al. 2004; Geddes et al. 2004; Mangles et al. 2004), density ramping injection (Geddes et al. 2008), density transition injection (Schmid et al. 2010), injection by colliding lasers (Faure et al. 2006), ionization injection by colliding lasers (Chen et al. 2006), and ionization-induced injection (Oz et al. 2007; Clayton et al. 2010; McGuffey et al. 2010; Pak et al. 2010) (we use ionization injection to abbreviate ionization-induced injection in the following). The idea of ionization injection is to utilize the ionization threshold of the inner shell of some specific heavy elements to control the initial position of the injected electrons. Electron beams produced by ionization injection are considered to have low emittances but large energy spreads (Pak et al. 2010). Later, the injector-accelerator LWFA scheme was proposed to

avoid continuous injection in the ionization injection scheme (Liu et al. 2011; Pollock et al. 2011). In this scheme, the injector is filled with a helium–nitrogen mixed gas where ionization injection takes place, and the accelerator contains a pure helium gas to provide acceleration without injection.

Here we carefully study the injector–accelerator LWFA scheme by simulation and propose a properly tailored density profile of the gas target in order to produce high-quality electron beams with small energy spread down to 1–2% in FWHM. Two-dimensional ($2\frac{1}{2}$D) particle-in-cell (PIC) simulations using the code OSIRIS (Fonseca et al. 2002) show that the injector-accelerator LWFA scheme exhibits an excellent performance once the parameters, such as the plasma density, the nitrogen concentration, the density up-ramp length, and the laser intensity and power are optimized. The density up-ramp length of the gas target in the injector is found to be critical to the beam monochromatism due to the 'bubble shrinking'(or accordion) effect (Katsouleas 1986). In addition, the self-focusing of the laser is found to clamp the injection in the injector flat top region. The highest quality electron beam produced by this scheme in our simulations is 350.3 MeV in energy, $\Delta E/E = 1.62\%$ in energy spread (FWHM), and 210 mm · mrad in normalized emittance.

2. General ideas of ionization-induced injection

Studies on laser wakefield show that a laser pulse can excite bubble-like plasma wake (Pukhov and Meyer-ter Vehn 2002; Lu et al. 2006a,b, 2007) with a phase velocity close to the group velocity of the laser in plasma if the pulse duration is about the plasma wave period and the laser intensity is highly relativistic, i.e. the normalized vector potential $a_0 = 0.85(I\lambda_0^2/10^{18}[\mathrm{W\cdot cm^{-2}\mu m^2}])^{1/2} > 1$, where I is the laser peak intensity and λ_0 is the laser wavelength. With such relativistic laser intensity, the plasma electrons are pushed outward while the ions still remain stationary because of their much higher mass. Consequently, a bare ion column is created to provide electrons with focusing and acceleration forces owing to the nonlinear plasma wakefield, which is referred to as plasma waves in the bubble regime. In this regime, self-injection of background plasma electrons occurs, which can produce quasi-monoenergetic electron beams (Faure et al. 2004; Geddes et al. 2004; Mangles et al. 2004; Tsung et al. 2004). The production of mono-energetic electron beams can occur from a variety of mechanisms, including phase space rotation (Pukhov and Meyer-ter Vehn 2002; Tsung et al. 2004; Lu et al. 2007), clamping due to beam loading, and the evolution of the bubble (Lu et al. 2007). One of the drawbacks of this scheme is that the electrons that are trapped in the back of the bubble have large transverse momentum (Lu et al. 2007).

A recent idea that might lead to lower emittance beams is ionization injection. Electrons ionized inside the wake (near the null of the E_z-field) are easier to trap. Ionization injection occurs when a gas with a large difference of ionization potential between the outer shell and inner shell electrons, such as nitrogen, is used. For nitrogen, two K-shell electrons are ionized by the optical field ionization close to the barrier suppression ionization threshold intensity, $I_{BS} \simeq 10^{19}\,\mathrm{W/cm^2}$ (the ionization potential of 552 eV to produce N^{6+} and the ionization potential of 667 eV to produce N^{7+}), whereas L-shell electrons are ionized below the intensity of $I_{BS} < 10^{17}\,\mathrm{W/cm^2}$ (the ionization potential is 98 eV to produce N^{5+}) and can be considered pre-ionized by the leading front of the laser pulse before bubble formation. Hence, the inner shell electrons are ionized only near the peak intensity of the laser pulse, which is located near the bubble center on the propagating axis, where the wake potential is at the maximum (the electric field is at a null), and the expelling ponderomotive force of the laser pulse is at the minimum. Therefore, the emittance can be limited to the residual momentum and the initial radius of the electrons from the ionization process itself (McGuffey et al. 2010; Pak et al. 2010).

In our 2D PIC simulations, we use 41fs (FWHM), 800 nm laser pulse with a waist of 9 μm, and a focus at the entrance of the helium–nitrogen mixed gas (the beginning of the up-ramp). The gas density has a trapezoidal profile with the up-ramp length $L_1 = 200\,\mu\mathrm{m}$ and the flat top semi-infinite, as shown schematically in Fig. 1(a). We scan other parameters, i.e. nitrogen concentration $c\%$, electron density n_e, and the amplitude of the laser-normalized vector potential a_0 at the focus in order to find a correlation of beam quality with these parameters. In each case, the simulation runs until the dephasing length, and the beam quality is measured at the position where the beam has the minimum energy spread (i.e. L_4 in Fig. 1(a) is optimized).

Simulations show that the proper electron density n_e should be between 0.004 n_c and 0.008 n_c (in Gaussian-cgs units, $n_c = m_e\omega_0^2/4\pi e^2$, where ω_0 is the laser frequency times 2π, e is the unit charge, and m_e is the electron mass. So $n_c = 1.7449 \times 10^{21}\,\mathrm{cm^{-3}}$ for $\lambda_0 = 0.8\,\mu\mathrm{m}$, where λ_0 is the laser wavelength) and a_0 at focus should be between 1.5 and 3.0. If n_e were smaller than 0.004 n_c, there would not be self-focusing (Sun et al. 1987; Mori 1997) and the laser was quickly dissipated by diffraction. If n_e were larger than 0.008 n_c, the bubble size would be smaller than the laser spot size leading to an ill-formed bubble. If a_0 is lower than 1.5, we observe no K-shell ionization for nitrogen atoms and consequently no ionization injection occurs. Further, if a_0 is larger than 3.0, self-injection can occur and K-shell ionization would be too far forward in the wake. It should be mentioned that although $a_0 = 1.5$ is lower than the ionization threshold of nitrogen atoms, self-focusing increases a_0 to values larger than this threshold. The nitrogen concentration was chosen

https://doi.org/10.1017/S0022377812000098 Published online by Cambridge University Press

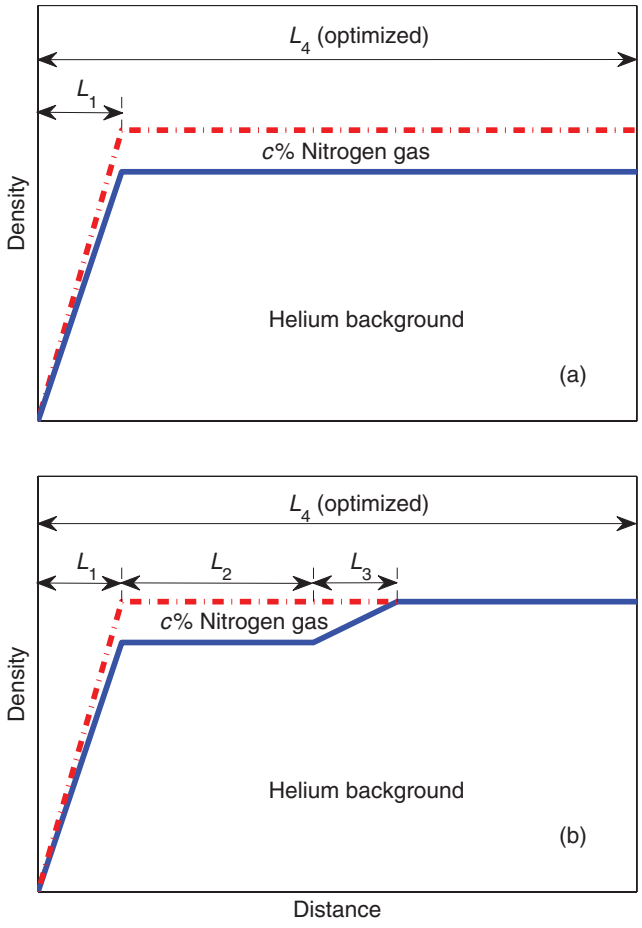

Figure 1. (Color online) Schematic electron density profile for (a) the single-stage, and (b) two-stage acceleration. The lines show the electron density profile. The laser incident from the left. In case (a), the target is helium–nitrogen mixed gas with a density up-ramp length L_1, and the nitrogen gas concentration is c%. In case (b), the first stage has a density up-ramp of length L_1 and a flat-top of length L_2. The density transition between the two stages has a length of L_3. L_4 is optimized so that the beam energy spread evolves to its minimum. The nitrogen gas concentration in the first stage is c%. The electron densities of the two stages are the same. Since a nitrogen molecule provides 14 electrons and a helium atom provides only 2, the gas pressure in the first stage is a bit smaller than that in the second stage.

to be lower than 10% so that the pre-plasma defocusing effect is reduced (Pak et al. 2010).

Figure 2 shows a typical picture of ionization injection. The nitrogen gas concentration is 0.5% in this case, and the total electron density is 0.004 n_c (i.e. 7×10^{18} cm^{-3}). The normalized laser peak amplitude $a_0 = 2.0$, which corresponds to a laser intensity of 8.6×10^{18} W/cm^2 and a laser power of 10.9 TW with $r_0 = 9\,\mu$m according to $P(\mathrm{GW}) \simeq 21.5(a_0 r_0/\lambda)^2$ (Esarey et al. 2009, p. 1231). Figures 2(e) and (f) show the density of the electrons ionized from helium and nitrogen, respectively, at $T =$ 16500 simulation unit (i.e. the propagating distance is 2101 μm). We can see the injected electrons gathering in the center of the bubble in Fig. 2(f), while the bubble in Fig. 2(e) is empty. This means that the nitrogen gas exclusively contributes to the injected electrons. Consequently, the injection mechanism here is solely due to ionization injection.

After propagating a distance, $L_d = (n_e/n_c)^{-3/2}\lambda_0$, where λ_0 is the laser wavelength, the accelerated particles, initially in the phase of the negative axial electric field or the accelerating phase, phase slip by π and enter the phase of the positive axial electric field or the decelerating phase. This phenomenon is called dephasing and L_d is the dephasing length (Lu et al. 2007; Esarey et al. 2009). This effect arises because the accelerated particles quickly have velocities larger than the phase velocity of the wake. So the dephasing length is estimated to be 3162 μm in case $n = 0.004\ n_c$. However, we found in the simulation that the dephasing length is largely reduced to 2101 μm because of a 'laser splitting' effect. The front of a laser photon decelerates to lower frequency (longer wavelength), which falls behind and enters the rear of the bubble (Mori 1997). In Fig. 2(h), we can see that the laser pulse splits into two end-to-end pulses after propagating 2101 μm and the axial E_1 field phase slips backward largely (Fig. 2(g)), which leads to an earlier dephasing. The 'laser splitting' effect largely reduces the acceleration distance and thus the accelerated electron energy. The electron energy spectrum at the reduced dephasing length is shown in Fig. 3(a), in which we can see that the maximum γ is 670 (i.e. energy 342 MeV). This beam has 14.5 pC, estimated by assuming the spot size in the translational invariant direction as same as in the other direction, with the mean energy of 170 MeV and the energy spread of 68% in FWHM.

3. Two-stage acceleration and plasma density-profile tailoring

3.1. Physical modeling

Ionization injection can produce a continuously injected electron bunch, which is harmful to beam monochromaticity. The question is: can we control ionization injection so that only a short electron bunch is injected and accelerated to high energy so that monoenergetic beam is produced?

One idea is to use a two-stage gas target. Another idea investigated here is to tailor the density profile. In our simulations, we use a two-stage gas target and tailor the gas density profile of the first stage. However, we find in many cases that the second stage is not needed. The gas density profile in our simulation is as follows. The first stage is a helium–nitrogen mixed gas with nitrogen concentration of around 0.5%, while the second stage is pure helium as shown in Fig. 1(b). The density transition between vacuum and the first stage, and between the first and second stages is assumed to be linear ramps with the length L_1 and L_3, respectively. The length of the density flat-top in the first stage (L_2) is 1000 μm scale. The length of the second stage is assumed to be infinitely long so that we can measure beam quality at

https://doi.org/10.1017/S0022377812000098 Published online by Cambridge University Press

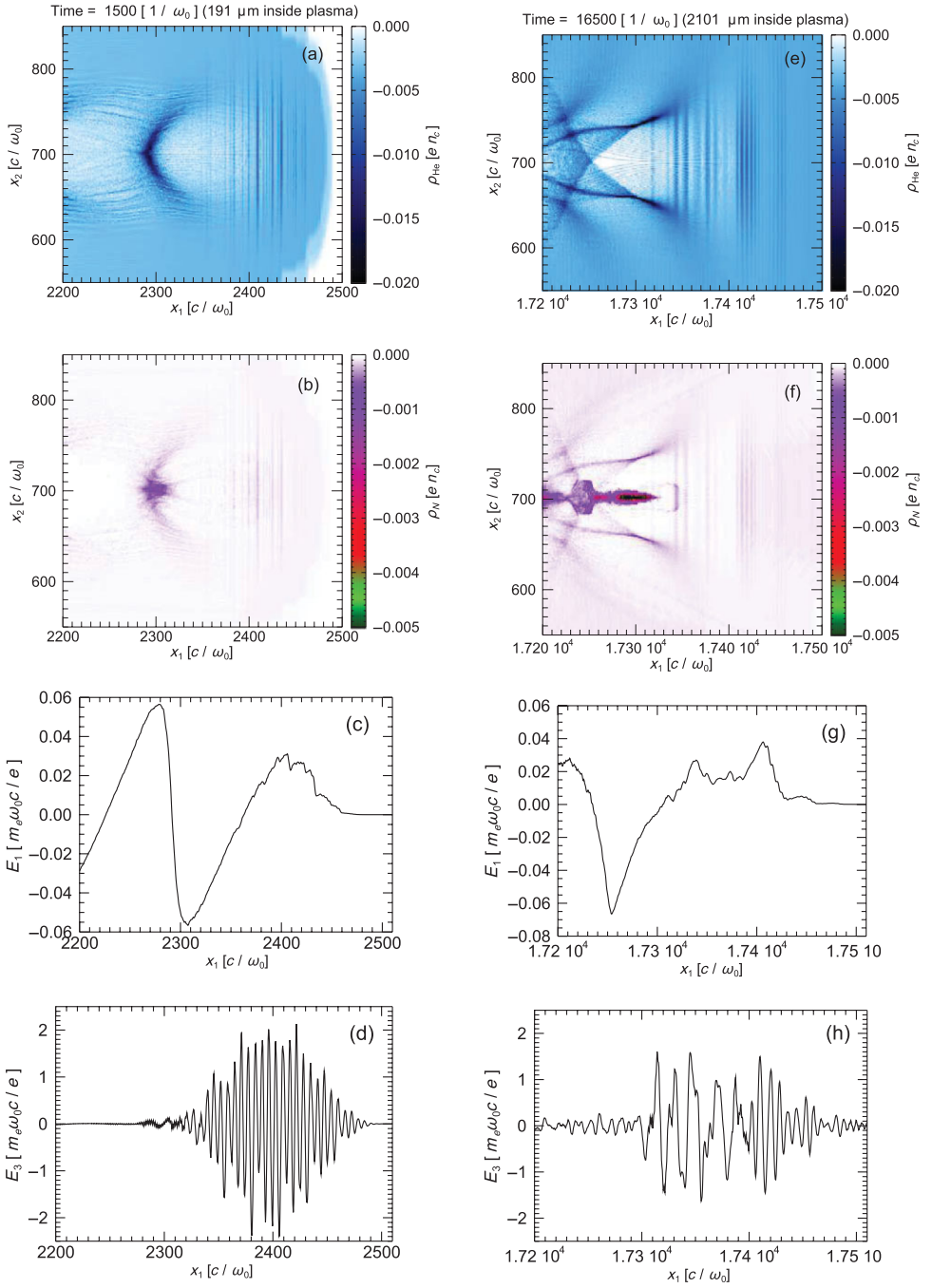

Figure 2. (Color online) The laser wakefield and bubble structure at two different time steps. Figures (a)–(d) are that at time 1500 (propagating distance 191 μm) and (e)–(h) are that at time 16 500 (propagating distance 2101 μm). (a) and (e) are the density maps of electrons that are ionized from the helium gas, and show no injection, while (b) and (f) represent those ionized from the nitrogen gas, and apparently show electrons injected in the bubble center. These injected electrons are ionized from the K-shell of nitrogen atoms. (c) and (g) show the corresponding axial longitudinal electric field E_1, and (d) and (h) are the axial laser electric field E_3. The charge densities are normalized to en_c, where e is the unit charge and the critical plasma density $n_c = 1.7449 \times 10^{21}\,\mathrm{cm}^{-3}$ in this case. The electric fields are normalized to the reference laser electric field $E_0 = m_e\omega_0 c/e = 4.02 \times 10^{12}\,\mathrm{V/m}$.

an optimized position (i.e. at a position where the beam evolves to the minimum energy spread). We neglect the influence of the exit of the gas target. The electron densities of both stages are 0.004 n_c (i.e. $7 \times 10^{18}\,\mathrm{cm}^{-3}$). The laser is S-polarized, and is 800 nm in wavelength. The profile is assumed to be Gaussian spatially, and sine-square temporally. The laser beam waist is $\sim 9\,\mu m$ and pulse duration is $\sim 41\,fs$ in FWHM. The normalized vector potential a_0 is fixed to 2.0, which corresponds to a moderate laser intensity of 10.9 TW.

3.2. Parameter scanning to minimize the energy spread

The simulation results indicate that the length of the electron density up-ramp of the first stage (L_1) is critical to beam monochromaticity. The nitrogen concentration in the first stage is also important. The length of the

https://doi.org/10.1017/S0022377812000098 Published online by Cambridge University Press

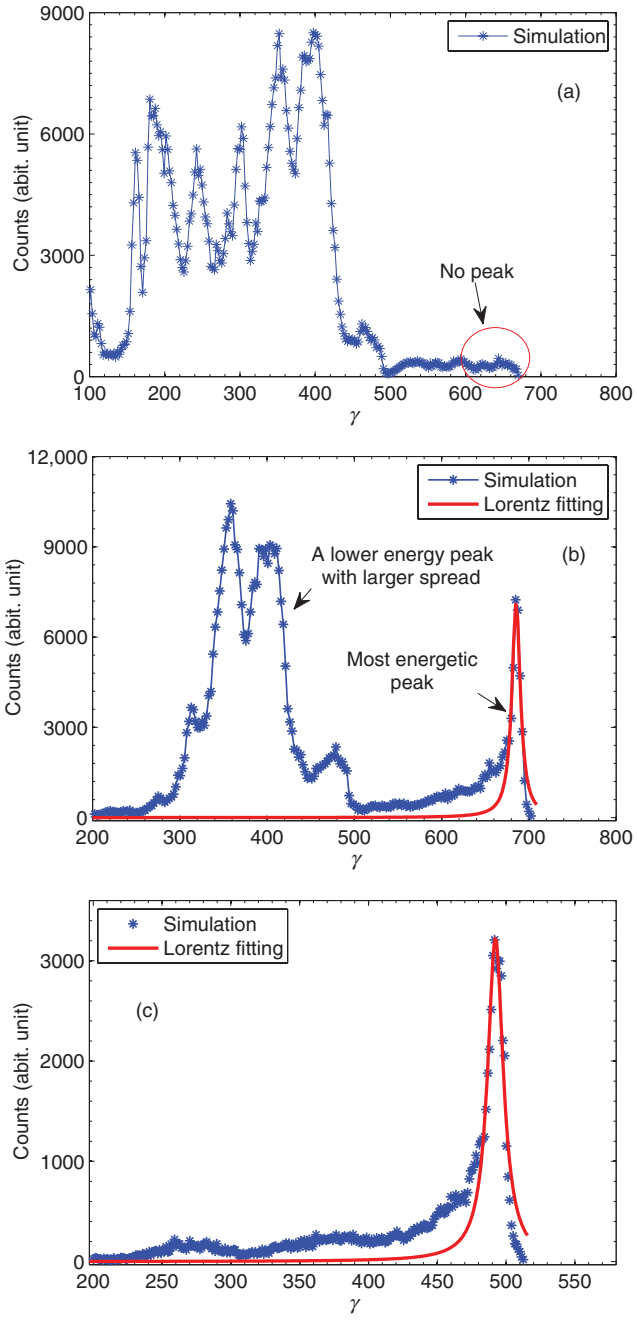

Figure 3. (Color online) Electron beam energy spectra correspond to (a) single-stage with same parameters as in Figs. 2(e)–(h), (b) two-stage with $L_1 = 135\,\mu$m in Fig. 4, and (c) $L_2 = 400\,\mu$m in Fig. 5. There is no peak in the range around $\gamma = 600$–700 in (a) because the gas density profile is not properly tailored. In (b) there is a peak with energy spread of 1.62% near $\gamma = 700$ and other relatively low peaks with larger energy spread and charge. In order to remove the low energy peaks in (b), we adjust L_2 to 400 μm so that only a single peak is obtained in (c). The acceleration distances (L_4) for above spectra are (a) 2100 μm, (b) 2037 μm and (c) 1337 μm.

density flat-top in the first stage (L_2) has minor importance. All these parameters are schematically shown in Fig. 1(b). In each simulation, L_4 is optimized so that the beam evolves to its minimum energy spread.

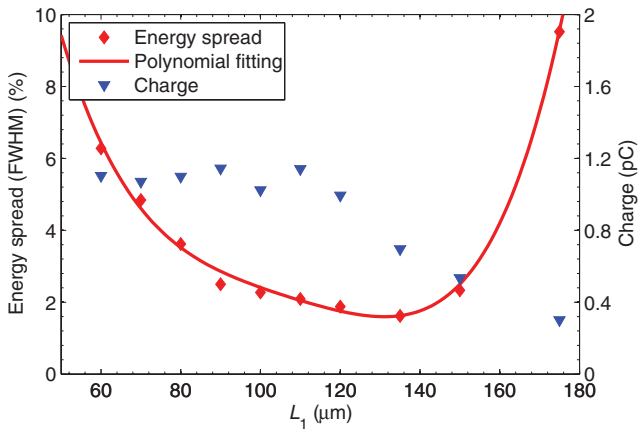

Figure 4. (Color online) The energy spread (the diamonds) and the charge (the triangles) of the most energetic spectral peaks vs. L_1 with the density profile shown schematically in Fig. 1(b), where $L_2 = 1000\,\mu$m, $L_3 = 100\,\mu$m and $c\% = 0.5\%$ in these cases. All the data are collected with the optimized acceleration distance L_4, which varies from 1100 to 1200 μm in different cases. The red diamonds show a minimum energy spread at $L_1 = 135\,\mu$m, of which energy spectrum is shown in Fig. 3(b). For L_1 larger than 175 μm, the charge of the most energetic beam is too low that we can hardly see a peak in the spectrum, and consequently the energy spread goes very large.

3.2.1. Varying L_1 while keeping L_2 and $c\%$ constant. Let $L_2 = 1000\,\mu$m and $c\% = 0.5\%$, while L_1 ranges from 60 to 175 μm. Figure 4 shows the beam charge and energy spread versus L_1. We can see that the minimum energy spread is 1.62% in FWHM at $L_1 = 135\,\mu$m, the corresponding spectrum is shown in Fig. 3(b). For L_1 larger than 175 μm, the charge of the monoenergetic bunch drops down and the energy spread goes up swiftly so that the monoenergetic peak is hardly seen in the spectrum (Fig. 3(a) is just an example for $L_1 = 200\,\mu$m). We call this phenomenon the 'up-ramping improvement' in the ionization injection mechanism, which will be discussed in detail in Sec. 4.

3.2.2. Varying L_2 while keeping L_1 and $c\%$ constant. Let $L_1 = 135$ μm and $c\% = 0.5\%$, while L_2 ranges from 0 to 2000 μm. Figure 5 shows the beam charge and energy spread versus L_2, where the minimum energy spread 1.62% in FWHM is found at $L_2 = 1000\,\mu$m (spectrum shown in Fig. 3(b)).

Figure 5 plots the energy spread as a function of the length of the density flat top of the injector. The latter has some minor influence on the accelerated beam energy spread. Relatively longer L_2 is beneficial to minimize the energy spread. Simulations show higher energy at the optimized L_4 if L_2 is relatively longer. But there is saturation at $L_2 > 1000\,\mu$m because of the dephasing effect introduced in Sec. 2. At $L_2 \simeq 1000\,\mu$m, the optimized L_4 is very close to the dephasing length of 2101 μm.

3.2.3. Varying $c\%$ while keeping L_1 and L_2 constant. Let $L_1 = 135\,\mu$m and $L_2 = 1000\,\mu$m, while the $c\%$ ranges from 0.1 to 1.0%. Figure 6 shows the beam charge

https://doi.org/10.1017/S0022377812000098 Published online by Cambridge University Press

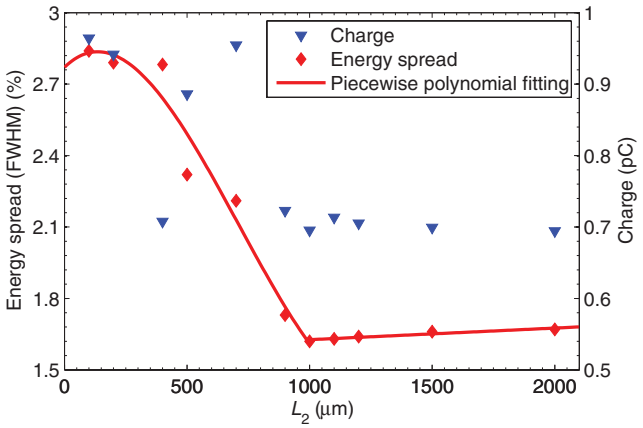

Figure 5. (Color online) The energy spread (the diamonds) and the charge (the triangles) of the most energetic spectral peaks vs. L_2 with the density profile shown schematically in Fig. 1(b)), where $L_1 = 135\,\mu m$, $L_3 = 100\,\mu m$ and $c\% = 0.5\%$ in these cases. All the data are collected with the acceleration distance L_4 optimized, and L_4 varies from 1200 to 2100 μm in different cases. The energy spectrum at $L_2 = 400\,\mu m$ is shown in Fig. 3(c).

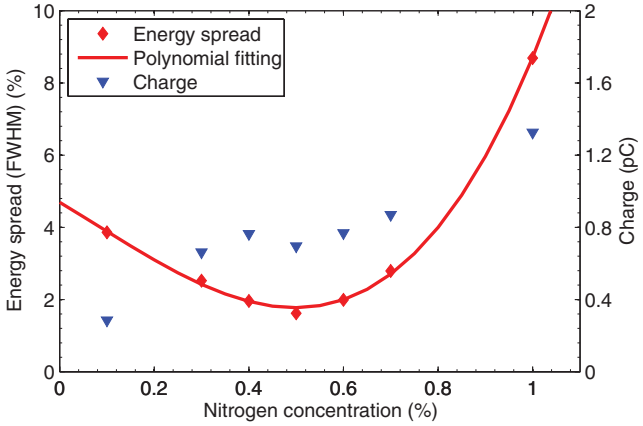

Figure 6. (Color online) The energy spread (the red diamond) and the charge (the blue triangle) of the most energetic peak in the spectrum vs. the nitrogen concentration $c\%$ with the density profile shown schematically in Fig. 1(b), where $L_1 = 135\,\mu m$, $L_2 = 1000\,\mu m$ and $L_3 = 100\,\mu m$ in these cases. All the data are collected with the acceleration distance L_4 optimized, and L_4 varies from 1200 to 2300 μm in different cases.

and energy spread versus $c\%$ and we can see that the minimum energy spread is 1.62% in FWHM at $c\% = 0.5\%$ (spectrum shown in Fig. 3(b)). This result may be natural because we have already optimized L_1 and L_2 with fixed $c\%$. We expect different optimized L_1 and L_2 for different $c\%$ in the later extensions of this work.

4. Discussion and conclusion

Section 3.2.1 indicates that the electron density up-ramp length in a region for which ionization injection can occur has an important impact on the electron beam energy spread. Detailed analysis shows that low energy-spread electron beams are injected at the end of the up-ramping. Figure 7(b) is a particle tracking of 300 random samples in the minimum energy spread case (i.e. $L_1 = 135\,\mu m$, $L_2 = 1000\,\mu m$, and $c\% = 0.5\%$). Energy evolutions of three groups of electrons are marked by three different colors. The red tracks show the energy evolution of electrons that are injected at the density profile turning point (i.e. the interface between the density up-ramping and the flat-top), which finally go to the highest energies and form a monoenergetic peak in the spectrum with small energy spread (the most energetic peak is in Fig. 3(b)). The green tracks show those electrons that have moderate energy, where only a small amount of electrons are contained. The blue tracks show the electrons that are injected deep inside the helium–nitrogen mixed region, which form a large population. In previous studies (Clayton et al. 2010; McGuffey et al. 2010; Pak et al. 2010), the main attention was paid on ionization injection from the mixed homogeneous gas density region, where the trapped electrons had trajectories similar to those of blue tracks and formed electron beams with a large energy spread. Thus, the present study suggests new possibilities to optimize the density profile to increase the energy gain and minimize the energy spread. In particular, by properly choosing L_1 in the inhomogeneous region, one may observe electron beams with 1% energy spread in future experiments.

The physics of the new injection mechanism can be explained as follows. Since the size of laser-driven bubble is inversely proportional to the plasma density (Lu et al. 2007), the bubble shrinks quickly at the time the laser enters the gas until it reaches the density flat-top (Fig. 7(a)). So once a nitrogen K-shell electron is ionized at the density up-ramping and is going to be trapped at the end of the bubble, the bubble size is reduced because the laser is going forward to a higher density region, and the electron runs out of the bubble and the trapping phase, i.e. the local phase velocity of the bubble may be controlled by the accordion effect (Katsouleas 1986) and be made larger than c. This situation happens all along the plasma density up-ramping except at the place near the density-profile turning point, where the bubble-shrinking terminates. This controls the injection starting point. The injection positions of these electrons are very close to each other, thus very small energy spread bunch is produced. Electrons injected deep inside the helium–nitrogen mixed gas (blue tracks) cannot catch up with those injected much earlier (red tracks). A small number of electrons shown by green lines are also injected close to the density profile turning point but do not go to the highest energy. It may be because of the random injection process. It is striking that there is an injection-free region corresponding to the propagating distance of 300–650 μm in Fig. 7(b). This injection-free region corresponds to the laser self-focusing region, as indicated by the evolution of the axial laser amplitude a_0 plotted in Fig. 8. Because of laser self-focusing, a_0 exceeds 3.0 in this region. The ionization injection may be occurring

https://doi.org/10.1017/S0022377812000098 Published online by Cambridge University Press

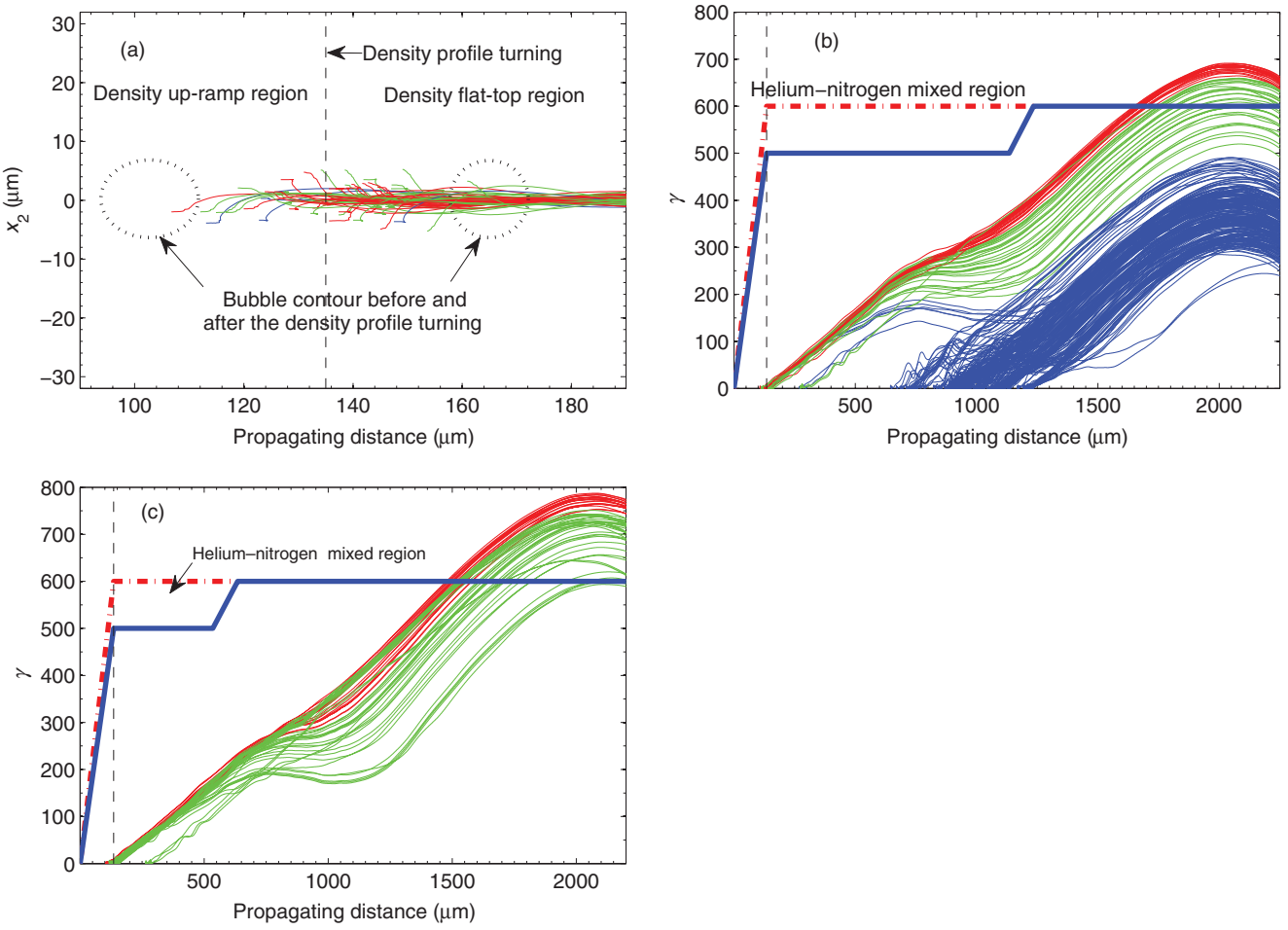

Figure 7. (Color online) Particle-tracking for cases (a) and (b): $L_2 = 1000\,\mu$m in Fig. 5 (spectrum in Fig. 3(b)), and (c): $L_2 = 400\,\mu$m in Fig. 5 (spectrum in Fig. 3(c)). The black dash lines represent the gas density profile turning point, and the thick solid blue and dot dash lines in (b) and (c) schematically show the gas density profile (the same as shown in Fig. 1(b)). The red thin lines show the tracks of electrons that reach the highest energies, while the green and blue lines show the tracks of electrons that gain moderate and the lowest energies, respectively. (a) shows the bubble shrinking phenomenon when passing through the density profile turning point. Comparing (c) with (b), we know that the low energy peak in Fig. 3(b), which corresponds to the blue thin lines in (b), is eliminated by changing L_2 from 1000 μm to 400 μm. This is simply because the injection of the low energy peak starts at 650 μm due to laser self-focusing (Fig. 8).

further forward in the bubble where the wake potential is low. In addition, if enough charge is trapped near the turning point, the beam loading reduces the wakefield, thereby clamps injection.

We note that the density gradient effect described here is different from the previously proposed density ramping injection in the self-injection scheme, where electron injection occurs at the density down-ramping and the wake bubble expands so that electrons on the tail of the bubble enter the bubble naturally (Geddes et al. 2008). Meanwhile, the density up-ramping injection happens in the ionization injection scheme only because the electrons are injected from the front in this scheme, and the bubble shrinking prevents injection until near the turning point.

The energy spectrum shows two main peaks for the minimum energy spread case ($L_1 = 135\,\mu$m, $L_2 = 1000\,\mu$m, and $c\% = 0.5\%$, Fig. 3(b)). The most energetic peak has a small energy spread, while the second peak has an energy spread larger than 10%. In order to remove the second peak, we choose another set of parameters, $L_1 = 135\,\mu$m, $L_2 = 400\,\mu$m, and $c\% = 0.5\%$, and the electron-tracking and the spectrum are shown in Figs. 7(c) and 3(c), respectively. One finds that a smaller L_2 can reduce the ionization injection process and remove the second peak. However, the energy spread is a bit larger as shown in Fig. 5.

To summarize, we have shown that the density up-ramping can control the ionization injection position and the energy spread. It is found that by properly choosing the density up-ramping length (shorter than 175 μm), the final energy spread goes down to 1–2% in FWHM. This phenomenon is distinct from ionization injection in mixed homogeneous gas. The up-ramping improvement only happens in ionization injection. In future, we plan on optimizing this process, better understanding the role of the laser focus and 3D effects.

https://doi.org/10.1017/S0022377812000098 Published online by Cambridge University Press

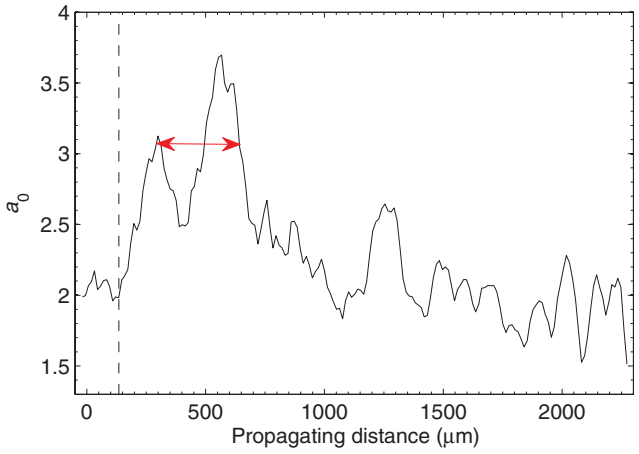

Figure 8. (Color online) Laser amplitude a_0 evolution corresponds to $L_1 = 135\,\mu m$. The other parameters, L_2 and $c\%$, do not have visible influence on laser evolution. The red double arrow shows that the injection-free region corresponds to propagating distance of 300 to 650 μm in Fig. 7(b). The initial laser amplitude is 2.0, while a_0 exceeds 3.0 at distance from 300 to 650 μm. This larger a_0 is harmful to ionization injection, thus an injection-free region is created. After 650 μm, a_0 goes lower than 3.0, and ionization injection happens again.

Acknowledgements

MZ and ZMS would like to thank Ricardo Fonseca at IST in Portugal and Frank Tsung at UCLA in the United States for their help on getting started with OSIRIS simulation. KN is supported by the Chinese Academy of Science Visiting Professorship for Senior International Scientists. This work is supported by the Natural Science Foundation of China (grants no. 10734130, 10935002, and 11075105), the National Basic Research Program of China (grant no. 2009GB105002), the National Science Foundation of China (NSFC) (grant no. 11175119), the US DOE (grant nos. DE-FC02-07ER41500 and DE-FG02-92ER40727) and US NSF (grant nos. PHY-0904039 and PHY-0936266).

References

Chen, M., Sheng, Z.-M., Ma, Y.-Y. and Zhang, J. 2006 Electron injection and trapping in a laser wakefield by field ionization to high-charge states of gases. *J. Appl. Phys.* **99**, 056109.

Clayton, C. E., Ralph, J. E., Albert, F., Fonseca, R. A., Glenzer, S. H., Joshi, C., Lu, W., Marsh, K. A., Martins, S. F., Mori, W. B. et al. 2010 Self-guided laser wakefield acceleration beyond 1 gev using ionization-induced injection. *Phys. Rev. Lett.* **105**(10), 105003.

Esarey, E., Schroeder, C. B. and Leemans, W. P. 2009 Physics of laser-driven plasma-based electron accelerators. *Rev. Mod. Phys.* **81**(3), 1229–1285.

Faure, J., Glinec, Y., Pukhov, A., Kiselev, S., Gordienko, S., Lefebvre, E., Rousseau, J.-P., Burgy, F. and Malka, V. 2004 A laser-plasma accelerator producing monoenergetic electron beams. *Nature* **431**(7008), 541–544.

Faure, J., Rechatin, C., Norlin, A., Lifschitz, A., Glinec, Y. and Malka, V. 2006 Controlled injection and acceleration of electrons in plasma wakefields by colliding laser pulses. *Nature* **444**(7120), 737–739.

Fonseca, R. A., Silva, L. O., Tsung, F. S., Decyk, V. K., Lu, W., Ren, C., Mori, W. B., Deng, S., Lee, S., Katsouleas, T. et al. 2002 Osiris: a three-dimensional, fully relativistic particle in cell code for modeling plasma-based accelerators. *Computational Science – ICCS 2002 Lecture Notes in Computer Science*, vol. **2331/2002**, pp. 342–351.

Geddes, C. G. R., Nakamura, K., Plateau, G. R., Toth, C., Cormier-Michel, E., Esarey, E., Schroeder, C. B., Cary, J. R. and Leemans, W. P. 2008 Plasma-density-gradient injection of low absolute-momentum-spread electron bunches. *Phys. Rev. Lett.* **100**(21), 215004.

Geddes, C. G. R., Toth, C., van Tilborg, J., Esarey, E., Schroeder, C. B., Bruhwiler, D., Nieter, C., Cary, J. and Leemans, W. P. 2004 Monoenergetic beams of relativistic electrons from intense laserplasma interactions. *Nature* **431**(7008), 538–541.

Katsouleas, T. 1986 Physical mechanisms in the plasma wakefield accelerator. *Phys. Rev.* A **33**, 2056–2064.

Liu, J. S., Xia, C. Q., Wang, W. T., Lu, H. Y., Wang, Ch., Deng, A. H., Li, W. T., Zhang, H., Liang, X. Y., Leng, Y. X. et al. 2011 All-optical cascaded laser wakefield accelerator using ionization-induced injection. *Phys. Rev. Lett.* **107**(3), 035001.

Lu, W., Huang, C., Zhou, M., Mori, W. B. and Katsouleas, T. 2006a Nonlinear theory for relativistic plasma wakefields in the blowout regime. *Phys. Rev. Lett.* **96**, 165002.

Lu, W., Huang, C., Zhou, M., Tzoufras, M., Tsung, F. S., Mori, W. B. and Katsouleas, T. 2006b A nonlinear theory for multidimensional relativistic plasma wave wakefields. *Phys. Plasmas* **13**(5), 056709.

Lu, W., Tzoufras, M., Joshi, C., Tsung, F. S., Mori, W. B., Vieira, J., Fonseca, R. A. and Silva, L. O. 2007 Generating multi-gev electron bunches using single stage laser wakefield acceleration in a 3D nonlinear regime. *Phys. Rev. ST Accel. Beams* **10**(6), 061301.

Malka, V., Fritzler, S., Lefebvre, E., Aleonard, M.-M., Burgy, F., Chambaret, J.-P., Chemin, J.-F., Krushelnick, K., Malka, G., Mangles, S. P. D. et al. 2002 Electron acceleration by a wakefield forced by an intense ultrashort laser pulse. *Science* **298**(5598), 1596–1600.

Mangles, S. P. D., Murphy, C. D., Najmudin, Z., Thomas, A. G. R., Collier, J. L., Dangor, A. E., Divall, E. J., Foster, P. S., Gallacher, J. G., Hooker, C. J. et al. 2004 Monoenergetic beams of relativistic electrons from intense laserplasma interactions. *Nature* **431**(7008), 535–538.

McGuffey, C., Thomas, A. G. R., Schumaker, W., Matsuoka, T., Chvykov, V., Dollar, F. J., Kalintchenko, G., Yanovsky, V., Maksimchuk, A., Krushelnick, K. et al. 2010 Ionization-induced trapping in a laser wakefield accelerator. *Phys. Rev. Lett.* **104**(2), 025004.

Mori, W. B. 1997 The physics of the nonlinear optics of plasmas at relativistic intensities for short-pulse lasers. *IEEE J. Quantum Electron.* **33**(11), 1942–1953.

Oz, E., Deng, S., Katsouleas, T., Muggli, P., Barnes, C. D., Blumenfeld, I., Decker, F. J., Emma, P., Hogan, M. J., Ischebeck, R. et al. 2007 Ionization-induced electron trapping in ultrarelativistic plasma wakes. *Phys. Rev. Lett.* **98**, 084801.

Pak, A., Marsh, K. A., Martins, S. F., Lu, W., Mori, W. B. and Joshi, C. 2010 Injection and trapping of tunnel-ionized electrons into laser-produced wakes. *Phys. Rev. Lett.* **104**(2), 025003.

Pollock, B. B., Clayton, C. E., Ralph, J. E., Albert, F., Davidson, A., Divol, L., Filip, C., Glenzer, S. H., Herpoldt, K., Lu, W. et al. 2011 Demonstration of a narrow energy spread, ∼0.5 gev electron beam from a two-stage laser wakefield accelerator. *Phys. Rev. Lett.* **107**(4), 045001.

Pukhov, A. and Meyer-ter Vehn, J. 2002 Laser wake field acceleration: the highly non-linear broken-wave regime. *Appl. Phys. B* (*Lasers and Optics*) **74**, 355–361, 10.1007/s003400200795.

Schmid, K., Buck, A., Sears, C. M. S., Mikhailova, J. M., Tautz, R., Herrmann, D., Geissler, M., Krausz, F. and Veisz, L. 2010 Density-transition-based electron injector for laser-driven wakefield accelerators. *Phys. Rev. ST Accel. Beams* **13**(9), 091301.

Sun, G.-Z., Ott, E., Lee, Y. C. and Guzdar, P. 1987 Self-focusing of short intense pulses in plasmas. *Phys. Fluids* **30**(2), 526–532.

Tajima, T. and Dawson, J. M. 1979 Laser electron accelerator. *Phys. Rev. Lett.* **43**(4), 267–270.

Tsung, F. S., Narang, R., Mori, W. B., Joshi, C., Fonseca, R. A. and Silva, L. O. 2004 Near-gev-energy laser-wakefield acceleration of self-injected electrons in a centimeter-scale plasma channel. *Phys. Rev. Lett.* **93**, 185002.